Journal of Hydrology 472–473 (2012) 77–89

Contents lists available at SciVerse ScienceDirect

Journal of Hydrology

journal homepage: www.elsevier.com/locate/jhydrol

Heat transport and temperature distribution during managed artificial recharge with surface ponds

Alexander Vandenbohede [a,*], Emmanuel Van Houtte [b]

[a] Dept. of Geology and Soil Science, Ghent University, Krijgslaan 281 (S8), B-9000 Gent, Belgium
[b] Intermunicipal Water Company of the Veurne Region (IWVA), Doornpannestraat 1, B-8670 Koksijde, Belgium

ARTICLE INFO

Article history:
Received 12 April 2012
Received in revised form 1 August 2012
Accepted 6 September 2012
Available online 25 September 2012
This manuscript was handled by Corrado Corradini, Editor-in-Chief, with the assistance of Renduo Zhang, Associate Editor

Keywords:
Managed artificial recharge
Groundwater
Heat transport
Temperature as tracer
Residence times
SEAWAT

SUMMARY

Managed Aquifer Recharge (MAR) is a well-established practice for managing groundwater reserves in a sustainable way. In this paper, we look at the influence of temperature variations of the infiltration water in the recharged aquifer. The paper focuses on MAR systems consisting of an infiltration pond surrounded by extraction wells. A number of different 2D configurations and an operational system in the Belgian dune area are investigated using field observations and numerical modelling with SEAWAT. Seasonally varying temperature in the infiltration water results in a zonation of subsequent lower and higher temperatures in the aquifer. The impact of infiltration water temperature in the aquifer is significant but restricted to the area between the pond and extraction wells, quickly decreasing farther from the infiltration area. Colder water during winter results in a decrease of infiltration capacity which can be as high as 1.5–2 times with respect to summer infiltration. Infiltration water temperature variations equally influence residence times of the infiltrated water. In general, residence times become smaller for water infiltrated during summer and larger for water infiltrated during winter. Infiltration and extraction rate, their ratios and seasonal variability, and location of extraction wells are all contributing factors to the impact of varying temperature of the infiltration water. Finally, it is shown that temperature provides only a rough proxy for residence times of solutes because of the important conduction of heat.

1. Introduction

Managed Artificial Recharge (MAR) systems are engineered systems which are used to augment groundwater resources, to reduce seawater intrusion or land subsidence, to store water, or to improve the quality of the water through soil-aquifer treatment (Bouwer, 2002). MAR provides a sustainable solution to meet water demand needs for drinking water production, agriculture, or industry while maintaining groundwater levels and safeguarding groundwater quality. Methods of MAR include river or lake bank infiltration, aquifer storage and recovery or surface infiltration via ponds. Different sources of recharge water can be used, e.g. surface runoff, storm water, reclaimed water or freshwater from desalination. Optimal operation of such systems requires knowledge about its operation under, in many cases, seasonally varying conditions.

In this paper, we focus on surface infiltration using ponds. A number of issues with regard to the design and operation of infiltration ponds are discussed in literature: design and engineering aspects (Bouwer, 2002), design optimisation (Eusuff and Lansey, 2004), general geochemistry (Gooren et al., 2011; van Breukel et al., 1998; Vandenbohede et al., 2009a), denitrification (Schmidt et al., 2011), saturated–unsaturated conditions and redox chemistry (Greskowiak et al., 2005; Massmann et al., 2006), fate of pollutants (Maeng et al., 2011; Stuyfzand, 1998; Stuyfzand et al., 2007; Wiese et al., 2011), residence times (Massmann et al., 2008; Vandenbohede et al., 2008) and clogging (Baveye et al., 1998; Hoffmann and Gunkel, 2011). Heat transport and temperature distribution in the recharged aquifer received little attention although it can influence cited topics. In most of the MAR systems using surficial infiltration, temperature of the recharge water varies seasonally. Alternating colder and warmer water is infiltrated influencing pore water temperature in the aquifer and temperature of the extracted water. Massmann et al. (2006) for example report temperature variations between 0 and 24 °C for an artificial recharge system in Berlin; Vandenbohede et al. (2009a) gives similar values for a system in the Belgian dune area. These temperature variations have a number of consequences for the operation and management of an MAR system.

Temperature variations causes change in hydraulic conductivity since pore water density and viscosity are temperature dependent. Temperature dependence of density is very small and is in most cases negligible. This is not the case for viscosity. Voss (1984) for instance gives the following relation between dynamic viscosity μ (kg/m s) and temperature T (°C):

* Corresponding author. Tel.: +32 9 2644652; fax: +32 9 2644653.
E-mail address: alexander.vandenbohede@ugent.be (A. Vandenbohede).

0022-1694/$ - see front matter © 2012 Elsevier B.V. All rights reserved.
http://dx.doi.org/10.1016/j.jhydrol.2012.09.028

$$\mu(T) = 239.4 \times 10^{-7} 10^{\frac{248.37}{T+133.15}} \quad (1)$$

It makes that hydraulic conductivity of the pond-aquifer boundary is lower during winter than during summer and this can be up to a factor 2. Less water can be infiltrated during winter which forms an important restriction for successful operation of an MAR system. Such an effect has been observed by Rorabaugh (1956) who argued that infiltration from a river to an aquifer was comparable in summer and winter although the gradient was different. Winslow (1962) described how the cone of depression caused by pumping near a river changed seasonally. Jaynes (1990) noted fluctuating infiltration rates from a pond during day and night and similar behaviour was reported from streams (Constantz et al., 1994; Constantz and Thomas, 1997; Constantz, 1998).

Temperature is an inexpensive though excellent tracer (Anderson, 2005). It can be used to study surface water – groundwater interaction. Slichter (1905) was probably the first to recognise the use of groundwater temperature as a tracer. He noted the relatively high groundwater temperatures because of induced infiltration from a pond in Long Island, New York. Suzuki (1960) and Stallman (1965) developed quantitative methods to calculate fluxes between groundwater and surface water from temperature measurements. Temperature as tracer can be used to study residence time of infiltrated water. This is an important parameter in the operation of MAR systems (Eusuff and Lansey, 2004; Massmann et al., 2008; Vandenbohede et al., 2008) since it influences health risk assessment (e.g. comparison with microbial die-off times and decomposition rates of pollutants), or progress of soil-aquifer treatment (e.g. re-mineralisation of infiltrated water).

Finally, temperature influences chemical reactions. Recharge water has in most cases a different composition than the pore water triggering a number or reactions. Massmann et al. (2006) and Sharme et al. (2012) showed that redox conditions under riverbank infiltration sites in respectively Berlin and Düsseldorf were largely dependent on seasonal temperature changes in the infiltrate. Prommer and Stuyfzand (2005) reported temperature dependent reaction rate of oxidation of pyrite during artificial recharge of an aerobic water in an anaerobic aquifer.

In this paper, we look at (i) temperature patterns in artificially recharged aquifers driven by seasonally varying temperature of the infiltration water, (ii) the possibility to use heat as a tracer in MAR systems, and (iii) influence of temperature on infiltration capacity for field case. Focus is on MAR systems consisting of a pond surrounded by extraction wells and it is considered that the pond is in contact with the groundwater (no unsaturated zone). This is achieved by simulating first heat transport for a hypothetical 2D case. The influence of different design parameters on the temperature distribution in the aquifer is evaluated. This provides a general framework before discussing heat transport for an operational MAR system in the Belgian dune area. Different temperature measurements (profiles and time series) are interpreted and heat transport is simulated. SEAWAT v4 is used for the simulation of heat transport.

2. Materials and methods

2.1. SEAWAT and heat transport simulation

The three-dimensional heat transport equation can be written as (Stallman, 1963):

$$\frac{\partial T}{\partial t} = \frac{\kappa_e}{\rho_b c_b} \nabla^2 T - \frac{\rho_F c_F}{\rho_b c_b} \nabla \cdot (Tq) \quad (2)$$

where T is temperature (°C), t is time (s), κ_e is a term that includes the bulk thermal conductivity of the rock–fluid matrix (W/(m °C)), c_b and c_F are specific heat of the rock–fluid matrix and the fluid (J/(°C kg)) respectively, ρ_b and ρ_F are the density of the rock–fluid matrix and fluid (kg/m) respectively and, q is the Darcy velocity or specific discharge (m/s). The first term on the right-hand-side of Eq. (2) represents conductive heat transport whereas the second term represents convective heat transport. SEAWAT version 4 (Langevin et al., 2007) is used to simulate solute and heat transport. This version 4 couples MODFLOW-2000 (Harbaugh et al., 2000) with the multi-species transport model MT3DMS (Zheng and Wang, 1999) in which the temperature is treated as one of the species. Fluid density and viscosity variations due to temperature changes are accounted for using the variable-density flow (vdf) process and viscosity (vsc) package. Simulation of heat transport with SEAWAT is based on the analogy between solute and heat transport which is discussed in detail by Wang and Anderson (1982), Anderson (2005), and Thorne et al. (2006). The application of SEAWAT to simulated heat transport has been verified by a number of bench mark problems and variable density and viscosity problems (Thorne et al., 2006, Dausman et al., 2010; Langevin et al., 2010)

Convection and conduction is mathematically analogous to advection and diffusion/dispersion for solute transport. The solute transport equation which is used in SEAWAT is manipulated to simulate heat transport (Thorne et al., 2006; Langevin et al., 2007):

$$\left(1 + \frac{1-\theta}{\theta} \frac{\rho_S c_S}{\rho_F c_F}\right) \frac{\partial(\theta T)}{\partial t} = \nabla \cdot \left[\theta \left(\frac{\lambda_b}{\theta \rho_F c_F} + \alpha \frac{q}{\theta}\right) \cdot \nabla T\right] - \nabla \cdot (qT) - q_s' T_s \quad (3)$$

θ is effective porosity (–), ρ_S is the density of the solid (kg/m^3), c_S is the specific heat capacity of the solid (J/(kg °C), α the dispersivity tensor (m), q_S' a source or sink (m^{-1}) and T_S is the source/sink temperature (°C). Specific relations are required to represent thermal equilibrium between the fluid and solid, heat conduction and a specific heat flux. There are no special considerations for representing advective heat transport (convection).

Equilibration of temperature between fluid and solid acts as a retardation coefficient and causes a temperature front to move slower than the average linear flow velocity. Therefore, a linear sorption isotherm is used in MT3D-MS' chemical reaction package and a thermal distribution coefficient K_{DT} (m^3/kg) is defined as:

$$K_{DT} = \frac{c_S}{\rho_F c_F} \quad (4)$$

This results in a thermal retardation R given by:

$$R = 1 + \frac{\rho_b}{\theta} K_{DT} \quad (5)$$

Thermal conduction is mathematically similar to solute transport process of molecular diffusion. The molecular diffusion coefficient used for the temperature species or also called the bulk thermal diffusivity D_T (m^2/d) is defined as:

$$D_T = \frac{\lambda_b}{\theta \rho_F c_F} \text{ with } \lambda_b = \theta \lambda_F + (1-\theta)\lambda_S \quad (6)$$

where by λ_F and λ_S (W/(m °C)) are the thermal conductivities of the fluid and the solid phase respectively. Bulk thermal conductivity is considered a linear combination of solid and fluid thermal conductivity.

2.2. Residence times calculation

Residence time, the time artificially recharged water is in the aquifer, is calculated by placing a large number of particles in finite-difference cells with artificial recharge. These particles are tracked towards the extraction well(s) and the travel time equals the residence time of each particle. A numerical scheme as used by Konikow and Bredehoeft (1978) was applied. The residence time is calculated as the advective age t_{adv} (d) of a particle:

$$t_{adv} = \int_{x_0}^{x_w} \theta \frac{dx}{q(x)} \quad (7)$$

where x (m) is the location on the flow line and $q(x)$ the Darcy flow velocity (m/d) at location x. Time to travel from the initial location x_0 in the pond to the well location x_w is determined for every particle. The velocity field to calculate particle displacement is updated according to the stress period as time progresses.

2.3. 2D MAR system

A hypothetical aquifer and MAR system is used to simulate a number of alternative infiltration pond designs. The aquifer has a thickness of 50 m, K_h is 20 m/d, K_v is 2 m/d and θ is 0.35. A 2D model with aquifer discretisation of 41 layers (20 layers of 0.5 m, 8 layers of 0.75 m, 4 layers of 1 m, 6 layers of 2.5 m, and 3 layers of 5 m), 1 row (1 m) and 37 columns (24 columns of 2.5 m, 8 columns of 5 m, and 5 columns of 10 m) is used. This is a cross-section situated perpendicular to an infiltration pond and infiltration occurs in the first two cells of layer 1. Water is extracted at a distance of 50 m with a screen between 10.75 and 14.5 m below surface. Infiltration and extraction rate is respectively 4 and 6 m^3/d. The model represents an infinitely long infiltration area with extraction on both sides.

A period of 5 years is simulated subdivided in stress periods of 3.65 days. For every stress period, temperature of the infiltration water changes according to a sine function:

$$T(t) = T_m + A \sin\left(\frac{2\pi t}{365} + \frac{\varphi}{365} 2\pi\right) \quad (8)$$

with mean temperature T_m of 15 °C, amplitude A of 10 °C and phase φ of 265 days. This means that the coldest water infiltrates at the beginning of January and the warmest water at the beginning of July. Initial temperature in the aquifer is 15 °C. Longitudinal dispersivity, horizontal transverse dispersivity and vertical transverse dispersivity are respectively 0.25, 0.025 and 0.0025 m. The molecular diffusion coefficient used for the temperature species is 0.113 m^2/d and thermal distribution coefficient is 1.763×10^{-4} m^3/kg. The third order total-variation-diminishing (TVD) scheme with upstream weighting is applied to solve for the advection/convection term while the generalised conjugate gradient (GCG) solver is employed for the non-advective terms.

From this reference scenario 1 five other variants are simulated (Table 1). The second scenario differs by the ratio of extraction to infiltration rate. Scenario 3 has a seasonal varying infiltration and extraction rate. During winter infiltration is less than during the rest of the year. The extraction to infiltration ratio is higher during winter. The mean infiltration and extraction rate over 1 year is the same as for scenario 1. Scenario 4 differs from 1 because of a higher extraction and infiltration rate but preserving the same ratio. Scenarios 5 and 6 have different positions of the screen: deeper in the aquifer for scenario 5 and farther from the pond for scenario 6. All scenarios are calculated with and without considering heat transport. In the latter case, the vdf and vsc packages are not used.

Table 1
Infiltration rate (Q_{inf}), ratio of extraction to infiltration rate (Q_{ext}/Q_{inf}), extraction well distance (r_w), and screen interval (d_w) for different hypothetical MAR scenarios.

	Q_{inf} (m^3/d)	Q_{ext}/Q_{inf}	r_w (m)	d_w (m)
Scenario 1	4	1.5	50	10.75–14.5
Scenario 2	4	1	50	10.75–14.5
Scenario 3	2.5[a]	2[a]	50	10.75–14.5
	4.75[b]	1.36[b]		
Scenario 4	6	1.5	50	10.75–14.5
Scenario 5	4	1.5	50	30–35
Scenario 6	4	1.5	75	10.75–14.5

[a] December–March.
[b] April–November.

2.4. St-André MAR system

Heat transport around a real-world infiltration system is studied in the Belgian dune area (Fig. 1). It comprises of two interconnected infiltration ponds with a combined surface area of 18,200 m^2 surrounded by a well battery of 112 extraction wells. Extraction wells have screens between 8 and 12 m below surface. The aquifer consists of Quaternary sand with a mean thickness of 30 m. It is underlain by a 100 m thick clay layer (Kortrijk Formation, Ieper Group) which is considered impervious in this study. The dune area has a width of about 2 km and contains a freshwater lens. It forms the only substantial freshwater reserve in the coastal plain.

Artificial recharge of the aquifer started in July 2002. Main motivation was to create a sustainable groundwater management (Van Houtte and Verbauwhede, 2005; Vandenbohede et al., 2009b). Use of MAR resulted in a sustainable solution. The recharge water is produced out of effluent from a nearby wastewater treatment plant using ultrafiltration (UF) and reverse osmosis (RO) (Van Houtte and Verbauwhede, 2008). It is permitted to infiltrate artificially 2.5 million m^3/y which is pumped up by the well battery. Additionally, the well battery is permitted to extract an extra 1 million m^3/y which is native dune water. Real values are lower than these permitted numbers. Average artificial infiltration rate for the last 3 years was 1.8 million m^3/y and extraction rate was 2.6 million m^3/y where there are important seasonal fluctuations in infiltration and extraction rates. What sets this system apart from other MAR systems is the very low mineralisation of the infiltration water because of the treatment with UF and RO. Mean total dissolved solids of the infiltration water is 50 mg/L compared with 500 mg/L for native dune water.

2.5. Observations St-André MAR system

Temperature profiles (temperature as function of depth) and time series (temperature at a given depth as function of time) are available. Temperature profiles are recorded by lowering a temperature measuring device very slowly (less than 10 m/h) in a well and recording temperature every second. It is assumed that the temperature of the water in the well is in equilibrium with the pore water in the sediments. Time series are recorded by putting a temperature measuring device at a certain depth in a well and recording the temperature every 30 min.

Temperature profiles were recorded in wells WP6, WP21, WP22, WP7 and P19 (Fig. 1). WP6 is located at the border of the western pond and profiles were recorded on 03/08 and 14/12 2007, 14/03 and 19/09 2008, and 21/01 and 05/06 2009. WP21 and WP22 are located between the western pond and the extraction wells and a single profile was recorded on 05/06/2009. WP7 is located south of the extraction wells and profiles were recorded on 17/03 and 19/09 2008, and 21/01 and 05/06 2009. These profiles are compared to well P19 located in the dune area but outside the influence of the water extraction. P19 is only affected by natural recharge and profiles were recorded on 04/02, 27/04 and 06/08 2010.

Time series are available during two separated periods of 1 year. First period goes from 09/03/2007 until 10/03/2008. Temperature was measured in the western pond, and in wells WP6, WP21 and WP22. In the latter two wells, time series were recorded at three different depth levels. Second period runs from 29/10/2010 until 29/12/2011. Time series were recorded in the pond and in wells WP24, WP23 and WP50. WP24 and WP23 are located between the eastern pond and the extraction wells and time series are

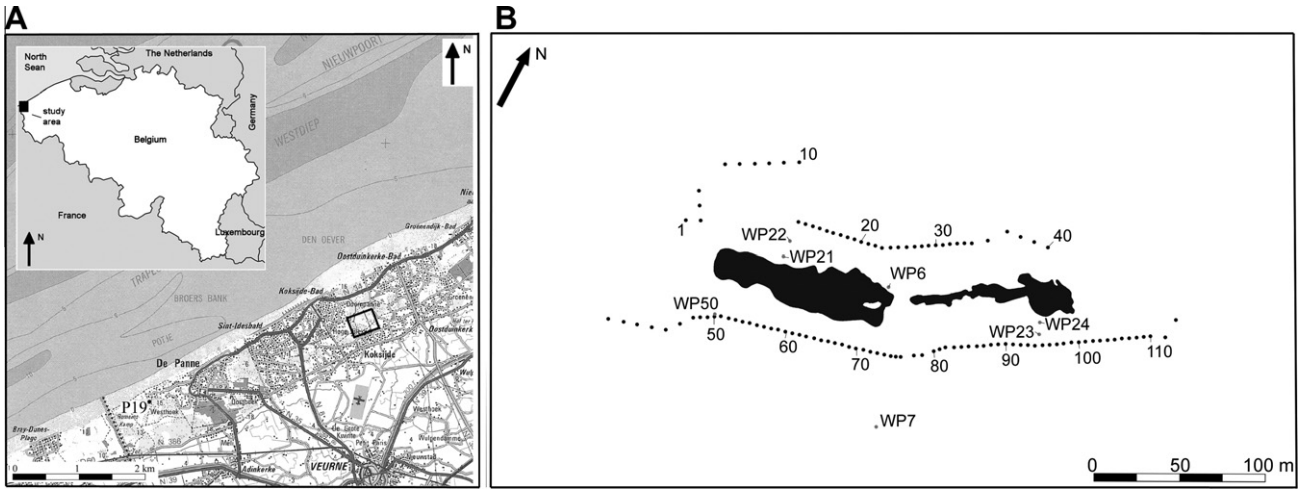

Fig. 1. Location of the study area in the dunes of the western Belgian coastal plain (A) and the model area with indication of the infiltration ponds, wells of the well battery (dots) and localisation of the observation wells (B). P19 is outside the MAR area and is indicated on the left figure. Wells of the well battery are numbered with an interval of 10.

recorded at two depth levels in WP24. WP50 is located in the line of extraction wells.

Time series of temperature of the infiltration and extraction water (i.e. combined volume of water from all extraction wells) is recorded from the start of the infiltration in 2002 and data on infiltration and extraction rates is available.

2.6. SEAWAT model St-André MAR system

A flow and transport model of the St-André MAR system was made by Vandenbohede et al. (2008) using the MOCDENS3D code. Based on this, a model using the SEAWAT code is made simulating transport of chloride and heat transport. SEAWAT is selected because of the multi-species capability and possibility to simulate heat transport. Other difference with the 2008 model is that the spatial resolution was increased from 10 to 5 m and that the thickness of the model layers was changed to have a better resolution in the upper part of the aquifer.

The model domain measures 1100 times 630 m^2 centred around the infiltration ponds (Fig. 1). It is subdivided in 180 columns and 86 rows. Width of rows and columns is 5 m except for the first and last 10 rows and columns. Of these, outer 5 rows and columns have a width of 20 m and inner 5 rows and columns have a width of 10 m. Aquifer thickness of 30 m is subdivided in 21 layers: upper two layers with a thickness of 0.25 m, 3 layers of 0.5 m, 7 layers of 1 m, 3 layers of 2 m and lower 6 layers of 2.5 m.

North and south boundaries consist of a constant head whereas the east and west boundaries are a no-flow boundaries. This is chosen because the model is situated along the dune – polder boundary. Due to the flow from the dunes towards the polder, east and west boundaries coincide with a flow line. Value for the constant head is 4 mTAW (0 mTAW is the Belgian reference level, 2.3 m below mean sea level) in both cases based on head observations and on a larger scale model comprising the polder, dunes, shore and sea (Vandenbohede et al., 2008).

Horizontal conductivity is 20 m/d for the upper part of the aquifer and 1 m/d for the lower 7.5 m of the aquifer. Vertical conductivity is 15 times smaller. Values are based on the calibration of the 2008 MOCDENS3D model and recent step-drawdown test data (unpublished data). Clay content of the sediments (Table 2; Lebbe, 1973) and geophysical borehole measurements (Vandenbohede et al., 2008) also supports a small decrease of conductivity for the lower part of the aquifer.

Table 2
Carbonate and clay content in% dry weight and resulting thermal distribution coefficient (K_{DT}) and bulk thermal diffusivity (D_T) for the different model layers.

Model layer	Carbonate (% dw)	Clay (% dw)	K_{DT} (m^3/kg)	D_T (m^2/d)
1–3	2–5	1–7	1.970×10^{-4}	0.089
4–18	5–10	<1	1.720×10^{-4}	0.113
19–21	7–12	1–5	1.763×10^{-4}	0.113

Artificial infiltration since the start in July 2002 is modelled until the end of 2011. This period is subdivided in stress periods of 3.65 days. Each stress period has a different infiltration and extraction rate and these values come from measurements. Two species are considered in the simulation: chloride concentration and temperature. Chloride is a conservative tracer in the dune area (Vandenbohede et al., 2009a) and is used for calibration purpose of the flow and transport model. Initial chloride concentration in the aquifer is 47.5 mg/L, which is a mean value for the dune aquifer. Chloride concentration in the infiltration water varies between 10 and 35 mg/L before May 2004, and is about 5 mg/L afterwards. Temperature of the infiltration water changes every stress period according to a sine function (Eq. (8)). The characteristics of this sine function are derived from the two periods of temperature observations in the ponds and are given in Section 3. Where natural recharge takes place (so not at the location of the ponds) a constant temperature boundary is used in the first layer. Temperature value for this boundary changes every stress period according to a sine function (Eq. (8)). Characteristics of this sine function are based on temperature variations near the water table as observed in WP7 and is given in Section 3. WP7 represents a situation without influence of the MAR system on the temperature profiles as will be shown later in the paper. Doing so, the natural variations of temperature in the aquifer is accounted for. No heat flux from the lower boundary is considered.

The thermal distribution coefficient and bulk thermal diffusivity (Table 2) are calculated based on carbonate and clay content given by Lebbe (1973) whereby the remainder of the sediment is considered to be quartz. Values for specific heat capacity and thermal conductivity for clay, quartz and calcite are taken from the SEAWAT manual (Langevin et al., 2007). Longitudinal dispersivity, horizontal transverse dispersivity and vertical transverse dispersivity are respectively 0.25, 0.025 and 0.0025 m. This is based on calibration of past models (e.g. Vandenbohede et al., 2008; Vandenbohede

and Lebbe, 2006) and a tracer test (Vandenbohede and Lebbe, 2003) in the Belgian dune area and coastal plain which all indicate relatively small values.

The third order total-variation-diminishing (TVD) scheme with upstream weighting is used to solve for the advection term while the generalised conjugate gradient (GCG) solver is employed for the non-advective terms.

Results of the flow and transport model are compared to time series of hydraulic head in observation wells, of chloride concentration in the extraction wells and of temperature observations in observation wells. Also a tracer test (Vandenbohede et al., 2008) was simulated and compared to the observations. The reader is referred to the Supplementary material with this paper for a detailed treatment of this calibration.

3. Results and discussion

3.1. Temperature distribution for the hypothetical MAR system

Fig. 2 gives for each scenario the temperature distribution in the aquifer at the end of December after 5 years of infiltration. Focus is on the first 100 m of the cross-section because the infiltration does not influence the aquifer farther from the pond. We look first to the reference scenario 1. A zonation in the temperature distribution is present in the aquifer which is the result of the subsequent infiltration of colder and warmer water. Temperature of the infiltration water at the end of December is 5 °C and cold water can be found in the immediate vicinity of infiltration pond. Farther from the pond, lateral away as well as deeper in the aquifer, temperature increases. This zone is influenced by the infiltration of warmer water during the previous summer. The actual water infiltrated during the previous summer has moved farther from the pond than this zone. Because of the retardation of temperature the term "influenced" is used here. Outside the zone of the warmer water, again colder water is found. This zone is influenced by the previous winter infiltration. But because of the longer time elapsed since previous winter infiltration and the important conduction of heat, this zone has become less apparent than the zone influenced by the infiltration of previous summer.

Fig. 3 gives temperature as function of depth every 2 months for the fifth year. Water with the highest temperature infiltrates at the beginning of July. During August, already cooler water infiltrates and the highest temperatures are found at a depth of 10 m. Consecutive colder water infiltrates over the next months and the zone with highest temperatures moves deeper in the aquifer: at a depth of 15 m at the end of October and at 19 m at the end of December. The temperature profile of August illustrates very well the temperature zonation which is present: top 5 m is influenced by very recent infiltration, high temperature at a depth of 10 m by previous summer infiltration and small temperatures at a depth of 20 m because of the previous winter infiltration. The upper part of the aquifer where pore water temperature is driven by temperature of recharge (natural or artificial) and atmospheric temperature variations is called the surficial zone (Parsons, 1970). For the reference scenario, depth of the surficial zone underneath the pond is 33.75 m (Table 3).

Fig. 4 gives temperature as function of distance from the pond in the first model layer during the fifth year. A similar evolution in zonation is visible as for the vertical temperature profiles of Fig. 3. Consider for instance the graph of August. Temperature of

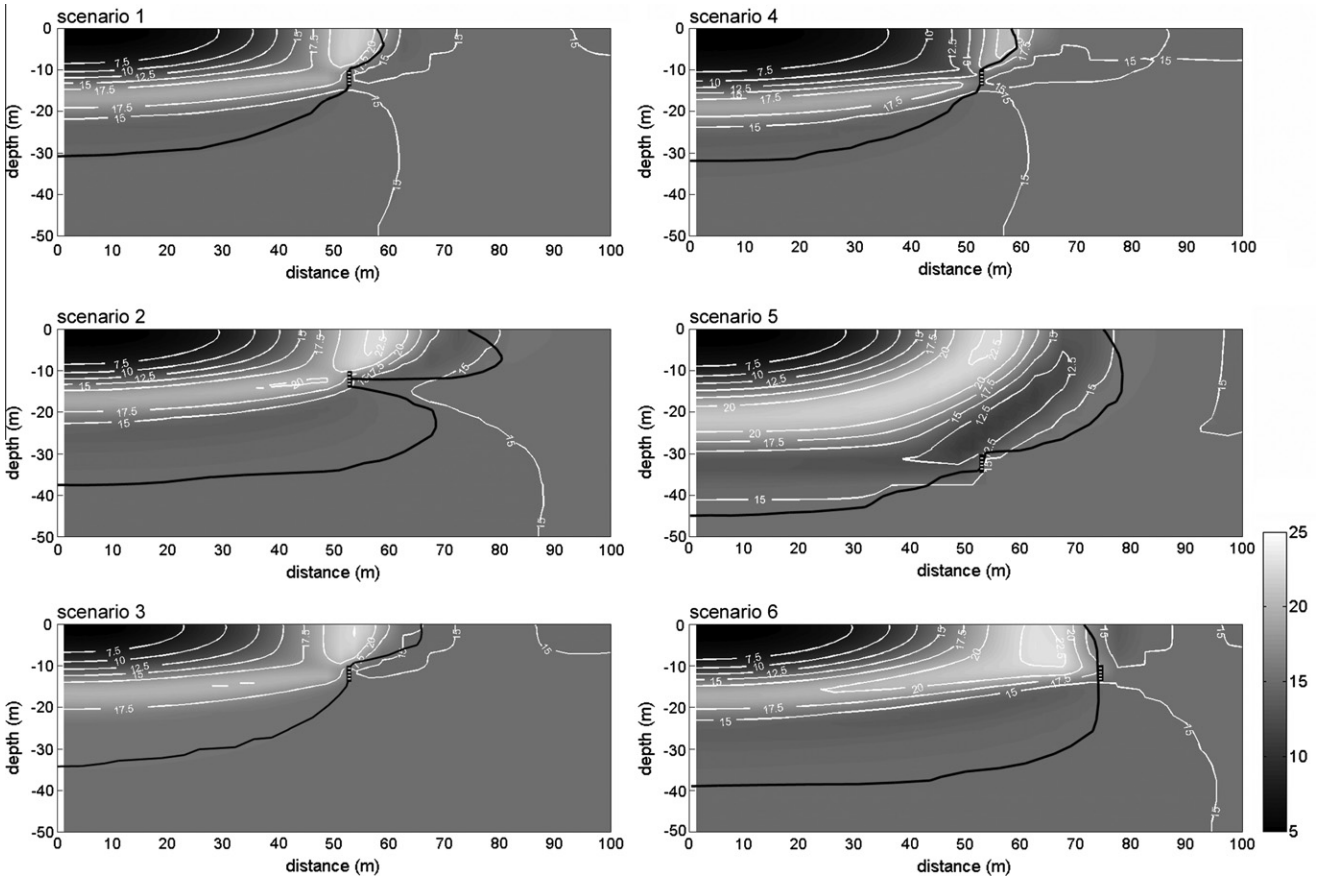

Fig. 2. Temperature distribution (°C) at the end of December after 5 years of infiltration for the different scenarios of the hypothetical MAR system. Well location is indicated and black lines represent the outline of the volume of infiltrated water after 5 years of operation.

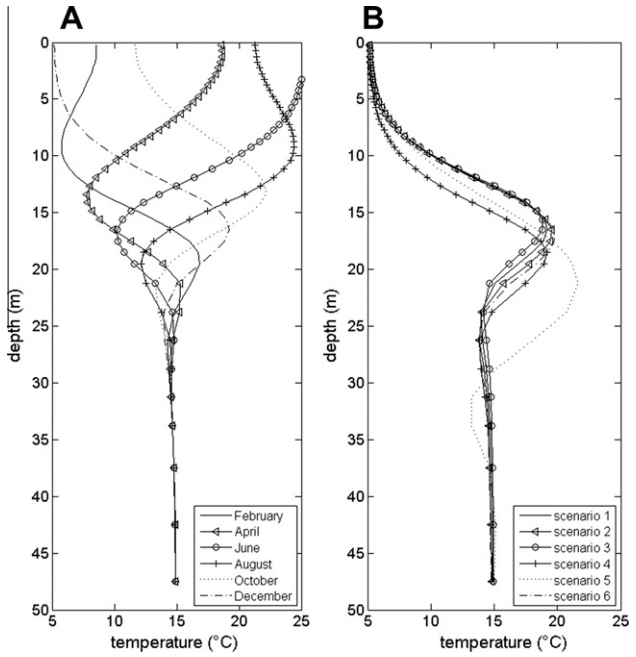

Fig. 3. Temperature as function of depth under the infiltration pond at the end of the indicated month (A) and temperature as function of depth at the end of December for the different scenarios (B).

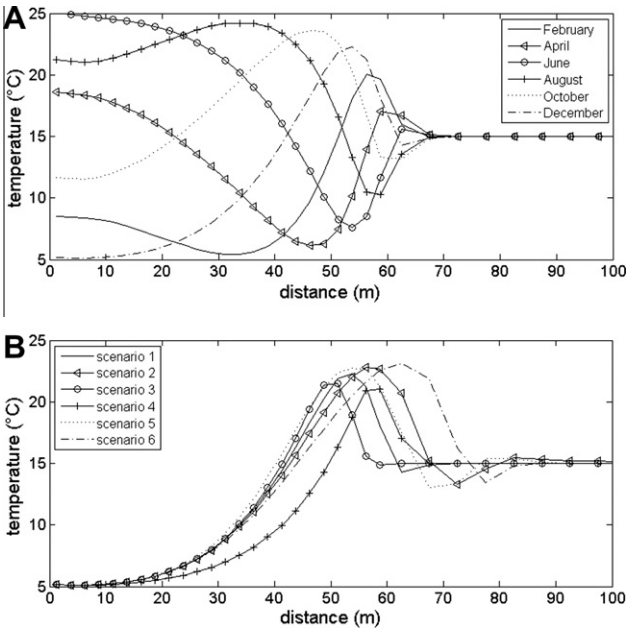

Fig. 4. Temperature as function of distance in the first model layer at the end of the indicated month (A) and the temperature as function of distance at the end of December for the different scenarios (B).

Table 3
Depth of the surficial zone (d_s), lateral extension of the pond temperature influence (l_{ext}), median of residence time of water infiltrated during winter or summer (m_w and m_s), median of residence time not taking into account heat transport (m), phase difference between temperature variations in the pond and the extraction wells for water infiltrated during winter ($\Delta\varphi_w$) and summer ($\Delta\varphi_s$) and head difference (Δh) in the pond between summer and winter for the five scenarios of the hypothetical MAR system.

	d_s (m)	l_{ext} (m)	m_w (d)	m_s (d)	m (d)	$\Delta\varphi_w$ (d)	$\Delta\varphi_s$ (d)	Δh (m)
Scenario 1	33.75	72.5	62.8	59.8	61.4	149.6	135.0	0.606
Scenario 2	33.75	92.5	72.4	67.8	71.3	157.0	142.3	0.594
Scenario 3	37.5	72.5	94.9	49.3	93.7[a] 51.8[b]	151.5	118.6	1.359
Scenario 4	37.5	72.5	41.1	37.6	39.4	109.5	93.1	1.017
Scenario 5	50	92.5	174.4	181.6	179.0	343.1	335.8	0.579
Scenario 6	37.5	87.5	101.8	97.1	99.3	226.3	206.0	0.567

[a] During winter (December–March).
[b] During summer (April–November).

the infiltration water has already decreased with regard to the maximum. At a distance of 40 m the influence of the summer infiltration is visible resulting in the high temperatures. At a distance of 60 m, temperature decreases and this zone is influenced by the infiltration of the previous winter. The maximum lateral influence is 72.5 m (Table 3).

The zonation has a larger lateral than vertical extension because of the flow pattern and flow velocities. Horizontal flow velocity is importantly higher than vertical flow velocity: most infiltration water flows laterally to the shallow extraction well. Testimony to that is the breach in the zone influenced by previous summer infiltration by colder water near the well. The area where pore water temperature is influenced by the infiltration is limited to the area where infiltration water is present.

Scenario 2 differs from scenario 1 by the ratio of the extraction to infiltration rate Q_{ext}/Q_{inf}. Decreasing the extraction rate (Q_{ext}/Q_{inf} equals 1) results in a larger volume of infiltration water in the aquifer since the same amount is infiltrated but less is extracted compared to scenario 1. Therefore, also the lateral influence of the temperature variation of infiltration water is increased to 92.5 m (Table 3 and Fig. 4). The zonation in temperature shifts laterally away from the well and the zone influenced by the previous winter infiltration becomes more pronounced. The depth of the surficial zone below the pond is the same as for the reference case (Fig. 3). Scenario 3 has a seasonally varying infiltration and extraction rate and this makes that the volume of recharged water in the aquifer changes slightly over the course of 1 year. The largest change concerning the temperature distribution is that there is an asymmetry in comparison with the reference scenario 1. The influence of summer infiltration is larger than the influence of the winter infiltration. Notice for example that in Fig. 2, the volume of recent infiltrated water is smaller than in case of scenario 1. The influence of the previous summer infiltration is larger than for the reference scenario. A larger volume of warmer water than colder water is infiltrated and this persists throughout the aquifer. Scenario 4 has the same Q_{ext}/Q_{inf} as scenario 1 but both infiltration and extraction rate are larger. The volume of aquifer with infiltration water is almost the same as for scenario 1. However, the higher rates results in a larger lateral influence on the temperature in the aquifer. The zone influenced by the recent infiltration of colder water has increased and the zone influenced by the previous summer infiltration is reduced. Because of the larger vertical flow velocities (higher infiltration rate) the depth of the surficial zone under the pond is increased to 37.5 m. Location of the well deeper in the aquifer (scenario 5) results in a surficial zone covering the complete aquifer thickness. Higher vertical flow velocities, because of the deeper location of the extraction well, make the surficial zone thicker. The deeper location of the extraction well limits less the extension of the influence of the infiltration pond in the upper part of the aquifer. The influence of the previous winter infiltration is more pronounced in comparison with scenario 1. Distinct zonation because of seasonal temperature variation is also apparent placing the extraction well farther from the pond (scenario 6). The lateral temperature influence is larger (87.5 m) than for the reference case. The volume of infiltrated water in the aquifer is larger than for the reference case. Because the larger distance of the

extraction well, infiltration water can flow deeper in the aquifer. Vertical flow velocities under the pond are larger which results in an increase of the surficial zone under the pond to 37.5 m.

Residence times are calculated by placing a large number of particles (2000) at the top of the first two cells of the first layer and tracking these towards the well. This was done for particles infiltrating during winter and summer for all scenarios (Table 3). Residence times are also calculated in case no heat transport is considered. The median m (d) of residence times of particles extracted by the well is calculated in each case.

Because hydraulic conductivity changes with temperature of pore water, also the velocity field varies seasonally influencing residence times. An increase in median residence time of 4.8% during winter is calculated for the reference scenario. Compared with the median residence time not considering heat transport, increase of median residence time during summer is 2.6% and decrease during winter is 2.3%. Lowering the extraction to infiltration ratio (scenario 2) results in a larger difference between residence times of winter and summer infiltration (6.4%). Especially winter infiltration shows a large difference (4.9 in comparison with 1.5%) with median residence times not taking into account heat transport. Seasonally varying infiltration and extraction rates results (scenario 3) in a large difference in median residence times for winter and summer infiltration. This is partially due to the changing rates but changing temperatures add to this: median residence times for summer infiltration are lowered (4.8%) and median residence times for winter infiltration becomes higher (1.3%). Preserving the extraction to infiltration rate but increasing both (scenario 4), results in no significant increase in difference in median residence times between winter and summer infiltration and median residence times not taking into account heat transport. However, residence times become smaller due to the higher rates and difference between median residence times of winter and summer infiltration increases to 8.5%. Scenario 5 shows the reverse: median residence times for summer infiltration is larger than for winter infiltration. This is due to the larger travel time from point of infiltration to the point of extraction. Residence times of individual particles range between 157 and 228 days for winter infiltration and between 160 and 248 days for summer infiltration. Consequently, median of residence time is influenced by much more varying (winter and summer) velocity fields than for the other scenarios. The effect of higher temperatures during summer infiltration and lower temperatures during winter infiltration on the conductivity are averaged. Relatively short residence times for the other scenarios are mainly influenced by only the velocity field during summer or during winter. The same applies partly for scenario 6 which shows the smallest difference between winter and summer infiltration. Locating wells farther from the pond (scenario 6) has only a very small impact on residence times in comparison with scenario 1.

Phase difference $\Delta\varphi$ (d) between temperature variations in the extraction water and pond water are calculated (Table 3). This phase difference is based on the highest and lowest point in the temperature variations of the extraction and infiltration water. These compare respectively with the phase difference of water infiltrated during summer ($\Delta\varphi_s$) and winter ($\Delta\varphi_w$). Such phase differences also represent a residence time but one must acknowledge the retardation of temperature. Retardation of temperature based on Eq. (5) and the used heat transport parameters is 2. Calculated retardation (based on ratio between residence times based on phase difference of temperature variations and calculated with particle tracking) is 2.4 for winter infiltration and 2.3 for summer infiltration for the reference scenario. Decreasing the extraction to infiltration rate (scenario 2) decreases calculated retardation. Seasonally varying extraction and infiltration rates (scenario 3) result in a calculated retardation of 1.6 and 2.4 for winter and summer infiltration respectively. Increase of rates but keeping the ratio constant (scenario 4) increases the calculated residence times to 2.7 and 2.5 for winter and summer infiltration respectively. Deeper wells (scenario 5) gives a calculated retardation of 1.9 and 1.8 for winter and summer infiltration respectively. Larger distance between pumping and extraction wells (scenario 6) decreases the calculated residence time slightly (2.2 and 2.1 for winter and summer infiltration) in comparison with the reference scenario.

Why these differences? Particle tracking takes into account only advection whereas convection as well as conduction determines heat transport. Or otherwise stated, particle tracing is only determined by the velocity field whereas temperatures are also mixed by conduction. This conduction is very important and mixing of temperature interferes with the calculation of residence times based on these temperatures. Consequently, different processes are compared when comparing the residence times based on particle tracking and temperature and this can lead to differences. This

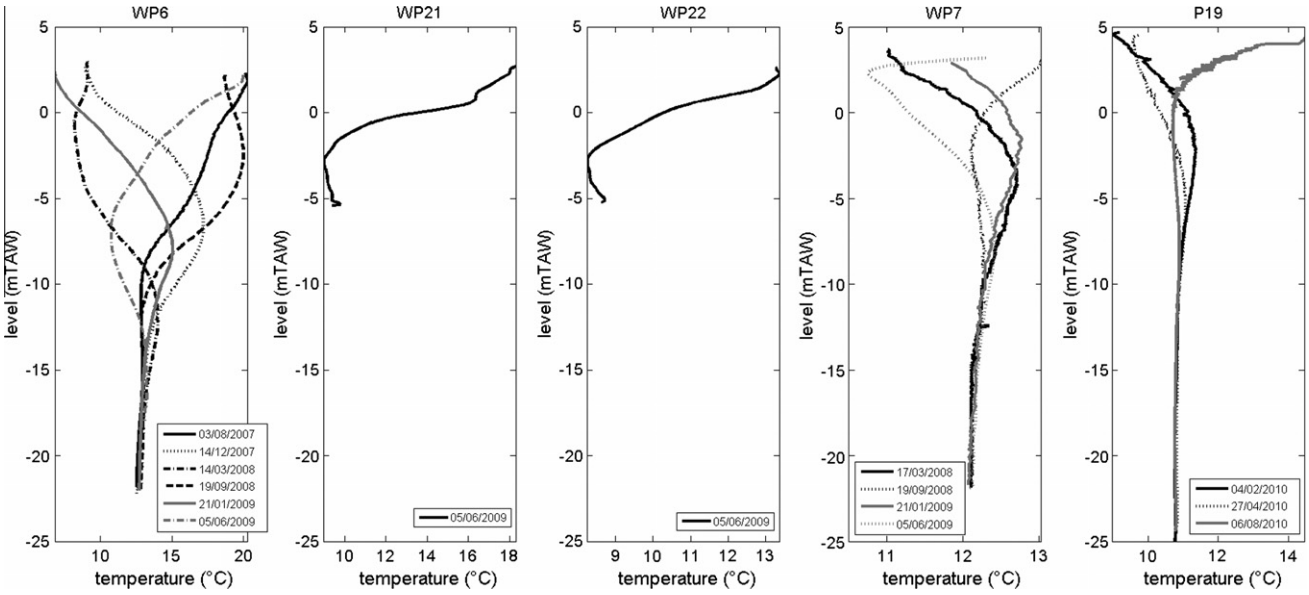

Fig. 5. Temperature profiles in the wells WP6, WP21, WP22, WP7, and P19.

Table 4
Mean temperature (T_m), amplitude (A) and phase (φ) for the sinus functions describing temperature at the water table as function of time for the well locations P19, WP6, and WP7.

	T_m (°C)	A (°C)	φ (d)
P19	10.75	2.25	210
WP6	13.5	7.5	250
WP7	12.1	1.1	210

Table 5
Mean temperature (T_m), amplitude (A), phase (φ) and phase difference ($\Delta\varphi$) with the pond water for the sinus functions describing temperature in the pond, extraction water and different levels in the observation wells.

	T_m (°C)	A (°C)	φ (d)	$\Delta\varphi$ (d)
Pond	13.5	9	265	–
Extraction water	13.75	3	155	110
WP6 1.6 mTAW	14.15	6.5	245	20
WP21 2.4 mTAW	14.25	7	240	25
WP21 0.4 mTAW	14	4	180	85
WP21 −3.5 mTAW	14	3.5	120	145
WP22 2.1 mTAW	13.75	5.5	190	75
WP22 0.5 mTAW	13.75	5.75	175	90
WP22 −3.8 mTAW	14	5	145	120
WP24 2.3 mTAW	13	7.75	240	25
WP24 −1.6 mTAW	13.25	7	200	65
WP23 −1.7 mTAW	13.25	7	200	65
WP50 −0.25 mTAW	12.75	6	120	145

puts some limitation of using heat as a tracer in a MAR system: expected retardation based on sediment properties is only a rough proxy. Finally, Table 3 shows that there is a higher phase difference for water infiltrated in winter than in summer, also for scenario 5, which means that the temperature variation in the well is not a sine function any more but becomes asymmetric.

Table 3 shows the head difference between winter and summer under the infiltration pond. Heads are higher in winter than in summer although the infiltration and extraction rate was constant during the year for each scenario with the exception of scenario 3. Head increase in winter is due to the lower conductivity of the aquifer under the infiltration pond because of the colder pore water. Head change varies from scenario to scenario but is significant. Because a real-world infiltration pond has an upper limit on the water level, it means that less water can be infiltrated during winter as was already pointed out in the introduction.

3.2. Field observations St-André MAR system

Fig. 5 shows temperature profiles in wells WP6, WP21, WP22, WP7 and, P19. P19 gives temperature profiles in a dune area where recharge is from precipitation only (Vandenbohede and Lebbe, 2011). In the 04/02 and 27/04 2010 profiles, temperature increases with depth in the upper part of the aquifer. Temperature at the water table is low because of the time of the year (winter and early spring). From a certain depth it decreases again until it reaches the long-term mean groundwater temperature which is 10.75 °C. The zone with higher temperatures between 5and 10 m depth is the response of the previous summer's high temperatures. The profile of 06/08 2010 shows decreasing temperature with depth until a minimum is reached. Deeper, temperature increases to the long term mean groundwater temperature. The minimum is the response of the low temperature of the recharge water during the preceding winter. The thickness of the surficial zone is 13.5 m. A sine function (Eq. (8)) was fitted through the temperature measurements at the water table. Table 4 shows the mean temperature, amplitude and phase. Based on this, highest temperatures are expected early September. In the study area, maximum yearly atmospheric temperature ranges between 30 and 35 °C and is in general reached at the end of June – early July. Minimum atmospheric temperature is generally observed in January and measures between 0 and −5 °C. Lag between water table and atmospheric temperatures is due to heat transport in the unsaturated zone.

Four profiles are available for WP7. These show a large similarity to P19 and thickness of the surficial zone is 14.5 m. A sine function (Eq. (8)) is fitted to the temperature variations near the water table. With respect to P19, WP7 show a slightly higher mean temperature and a lower amplitude (Table 4). This can be explained by a thicker unsaturated zone at location WP7. The phase difference is the same as for P19 indicating that atmospheric temperature variation is the main driving force. There is no indication of influence of the recharge pond on the groundwater temperature at that location. The thicker surficial zone can be explained by a larger vertical velocity because of the proximity to the extraction.

A different picture emerges from WP6, located at the border of the western pond. Mean temperature T_m at the water table (Table 4) is higher than for WP7 and P19. Amplitude of 7.5 °C is much larger than amplitude of WP7. Mean temperature and amplitude are comparable to the values for the recharge water which is given in Table 5. Thickness of the surficial zone is about 20 m which is significantly larger than the surficial zone observed in WP7 and P19. Obviously, temperature variations of the recharge water and the high vertical flow velocities influence temperature variation and thickness of surficial zone. Only one profile is available in WP21 and WP22 but this illustrates the temperature as function of distance from the pond. At 05/06/2009, temperature at the water table at WP6 is 20 °C. At WP21 and WP22 this is respectively 18.3 °C and 13.3 °C. At WP7, this is 12.3 °C. No measurements of the temperature in the pond water is available for June 2009 but this is about 21 °C using the parameters in Table 5. Consequently, temperature at the water table decreases away from the pond at that time. Although a zonation of temperature is expected as calculated with the hypothetical MAR system, temperature at the water table as function of distance shows also a decrease between pond and well position at the end of June (Fig. 4).

Fig. 6 shows the time series of temperature in the different wells and the ponds for periods 1 and 2. Fig. 7 gives time series of temperature of the extraction water. This is the temperature of the combined water from all individual wells of the well battery. A sine function (Eq. (8)) was also fitted through these time series and mean temperature, amplitude and phase are given in Table 5. With the exception of WP50, all time series can be approximated by a sine function. Mean temperature of the recharge pond is 13.5 °C and temperature varies with an amplitude of 9 °C. However, temperature of the pond water can be almost close to zero or as high as 30 °C during brief periods. Phase is 265 days which means that the highest temperature is recorded during the beginning of July. Lowest temperature is observed during the end of December – beginning of January. Temperature of the pond water is thus determined by the atmospheric temperature variation.

Mean temperature T_m for all observation wells between the pond and the extraction wells is between 13 and 14.25 °C showing the influence of the recharge water. T_m of the extraction water is also 13.75 °C. Individual extraction wells can show a different picture. T_m of WP50 for instance is noticeably lower. WP50 is located southwest of the infiltration pond in between the extraction wells. Time series in WP50 show an asymmetric variation as was also determined in extraction wells of the hypothetical MAR system. Phase difference between the temperature of pond water and extraction water is 110 days.

In WP6, T_m of the time series at level 1.6 mTAW (about 4.5 m below the bottom of the pond), is similar to that at the water table (Table 4) or of the pond water. The amplitude has decreased from 9 °C in the pond, 7.5 °C at the water table to 6.5 °C at the level of 1.6 mTAW. This decrease of amplitude is very well illustrated by

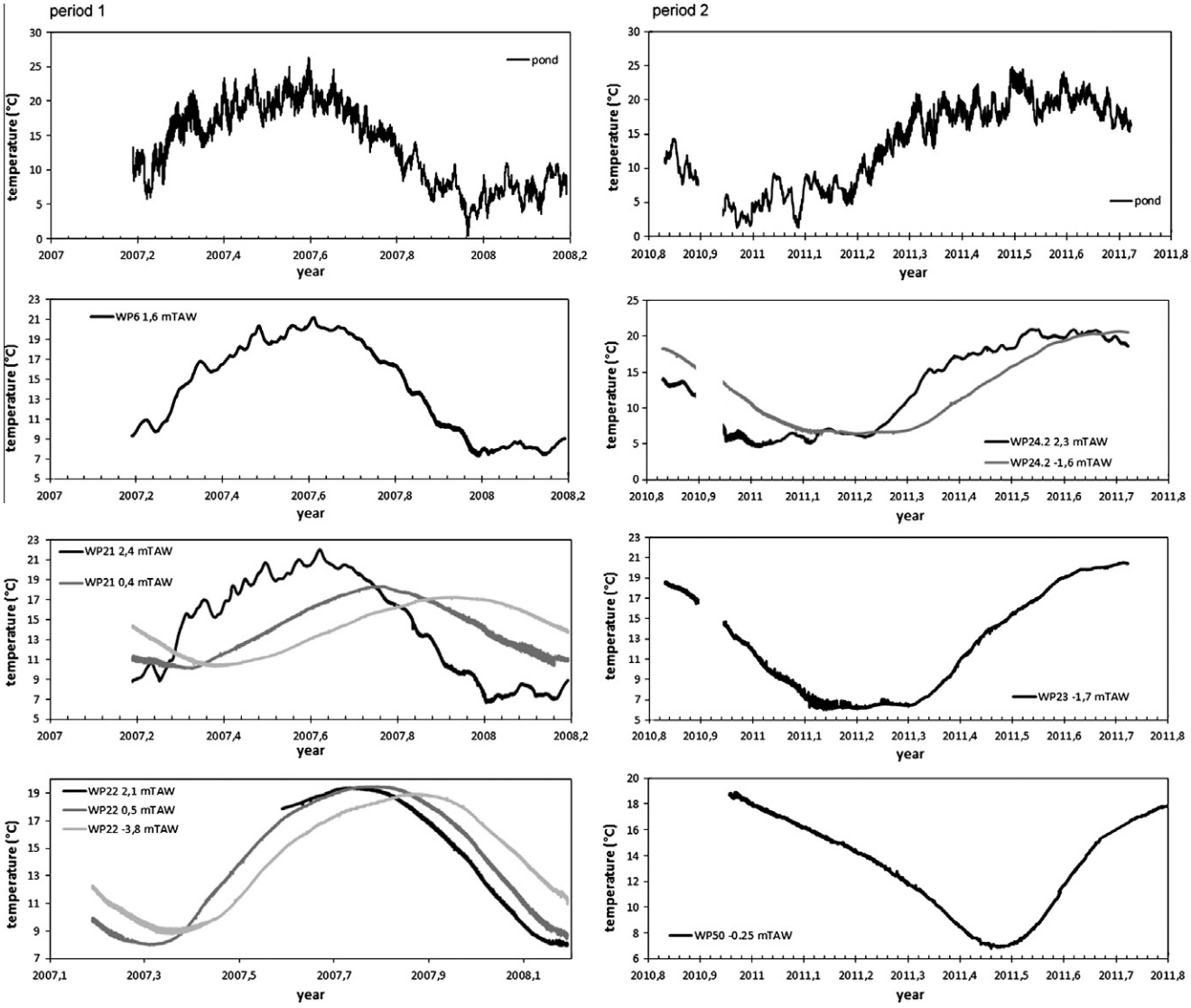

Fig. 6. Time series of temperature in the different wells during period 1 (left) and period 2 (right).

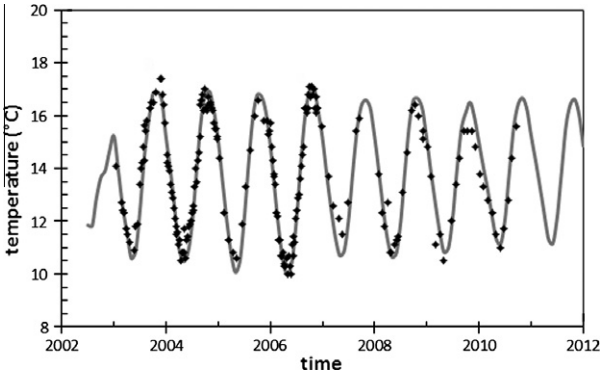

Fig. 7. Temperature in the extraction water. Full line is the simulation results and underlines the seasonal variation of the temperature.

the temperature profiles in WP6 (Fig. 5). There is a decrease of the phase: 265 days in the pond water, 250 days at the water table and 245 days at level 1.6 mTAW. This phase shift as function of depth is relatively small because of the high downward velocity. WP21 is at a distance of 7 m from the pond and the mean temperature at all three measurement levels is about the same. Amplitude and phase decreases with depth. The shallow observation point shows only 25 days of difference in phase with the pond water. This increases to 85 and 145 for respectively the middle and lowest observation pond. WP22 is located at a distance of 34 m from the pond and measurement on all three levels show about the same mean temperature and amplitude. The phase decreases again with depth. During the second period, WP24 and WP23 show the same pattern. The phase difference is less for these wells than for WP21 and WP22 which can be explained by the smaller distance between pond and extraction wells in that part of the well battery.

Small short-term temperature variations in the pond water are visible only in the shallow part of the aquifer. Such small variations are still observable in WP6 and the upper observation point of well WP21 and WP24. They are filtered out in the deeper observation points of WP21 and WP24 and not visible at all in wells WP22 and WP23. Conduction of heat smoothen these short-term variations very quickly and a more homogeneous temperature observation is obtained.

3.3. Influence on recharge capacity

Temperature range of almost zero to 30 °C result in a change of dynamic viscosity with a factor of 2.2 according to Eq. (1).

Consequently, also the hydraulic conductivity of the sediments changes with this factor and this has an implication on recharge capacity. Fig. 8 shows the effect of temperature of the recharge water during the first observation period. Level of the pond and recharge and extraction rate is given as function of time. During autumn and winter, recharge rate is smallest and remains pretty much constant. Extraction rate, however, increases. Despite this, the water level in the pond increases. Because of the lower temperature of the recharge water, less water can be recharged resulting in a higher water level. The effect increases during winter because of the increasing volume of colder water present in the subsurface. From April-May, both temperature of the recharge water and the recharge and extraction rate increase again. Result is a slightly higher water level but it is almost impossible to evaluate the impact of temperature. Increase in recharge rate should increase the water level whereas the increase of extraction and increase in temperature of the recharge water should decrease the water level. The same applies for the period June to September. Recharge and extraction rate decrease, temperature of the recharge water increases and the level in the pond also decreases.

Fig. 9 shows the ratio of extraction to infiltration rate for the different months of the years 2005 until 2011. The first few years of the artificial recharge are not shown because this must be considered as a start-up period for the system. The system has a mean ratio of 1.35 with a mean extraction rate of 2.66 million and a mean infiltration rate of 1.96 million m^3 during this period. For most years, this ratio is below 1.35 from May until November. From December until April, the ratio is well above 1.35. Recharge rate decreases during winter and early spring with respect to the extraction rate. This effect is especially apparent from 2006 onward. Decrease of rate during winter is only because of decrease of infiltration capacity.

3.4. Modelling St-André MAR system

Fig. 10 gives the calculated temperature distribution at the beginning of January and at the beginning of July according to model layer 1. At the beginning of January, cold water is present in the immediate surroundings of both infiltration ponds. Farther away from it warmer water is present: this is the influence of the water infiltrated during the previous summer. The reverse is observed during summer. Warm water is present in the immediate surroundings of the infiltration ponds and colder water, influenced by the previous winter infiltration, is present farther from the ponds. Outside this zone at some locations (e.g. between wells 23–36 and 75–87), still cold (January) or warm (July) water is present. This water is influenced by the previous winter or summer respectively. As was shown with the hypothetical MAR systems, the relative importance of difference zones in this zonation is determined by position of extraction wells and infiltration and extraction rates. Influence of older infiltration is found where the distance between pond and extraction wells is largest. Wells 1–10 illustrate this very well. The January simulation shows influences of previous year winter previous summer infiltration. The same, but with reverse temperatures is visible during summer.

Temperature variations due to the infiltration is limited to the area between infiltration ponds and extraction wells. This agrees with the results of the hypothetical MAR system.

Fig. 11 gives vertical cross-sections located through the eastern and western pond. Cross-sections at the beginning of January and the beginning of July are shown. January cross-sections through the eastern pond show the temperature zonation, with recently infiltrated cold water close to the pond and warmer water influenced by previous summer infiltration farther from the pond. As

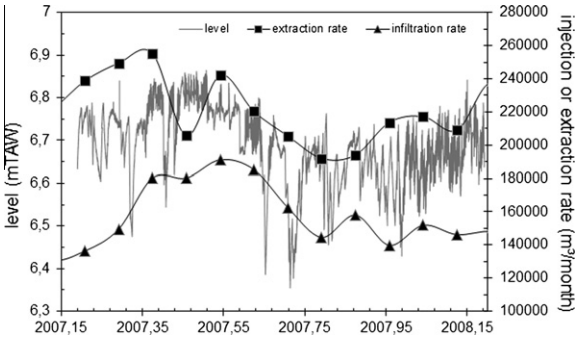

Fig. 8. Water level of the pond and recharge and infiltration rate as function of time during the first period of observations.

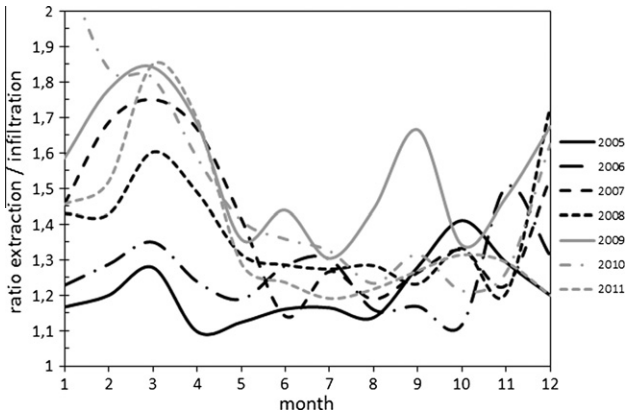

Fig. 9. Ratio between extraction and infiltration rate as function of the month of a year for the period 2005–2011.

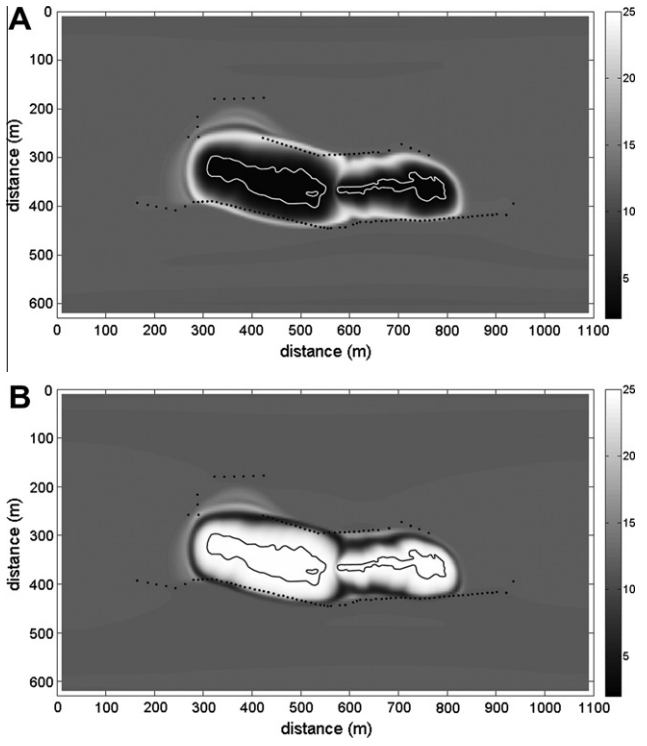

Fig. 10. Temperature distribution in the upper model layer at the beginning of January (A) and at the beginning of July (B) of 2012. Locations of the wells and the infiltration ponds are indicated.

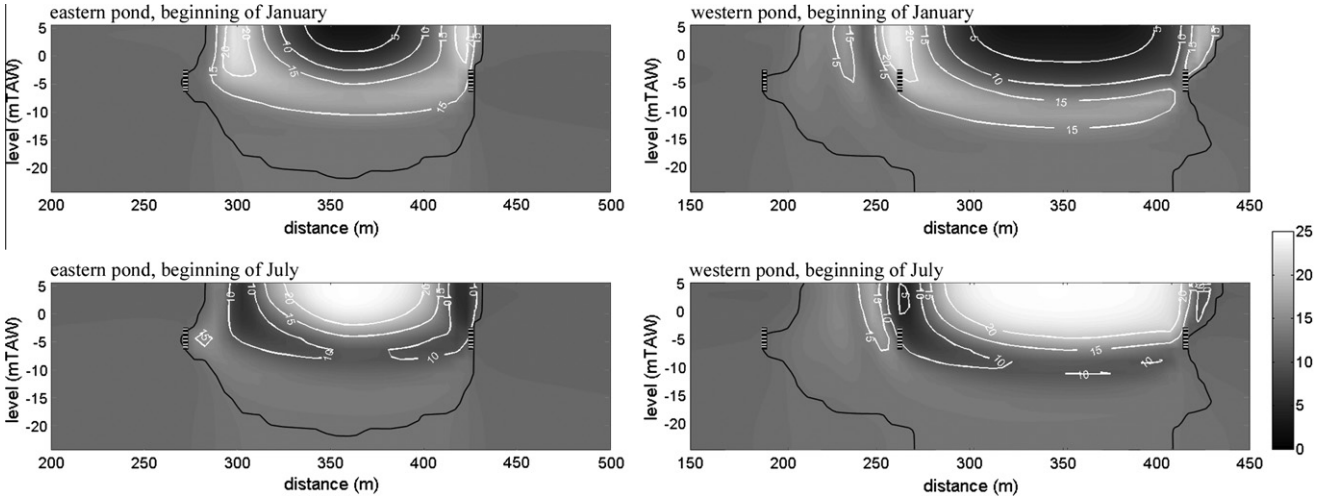

Fig. 11. Temperature distribution in vertical cross-sections through the aquifer at beginning of January and beginning of July of 2012. Cross-sections run through the eastern (x is 700 m) and the western pond (x is 420 m). Location of the wells and the extension of the volume of infiltration water (black line) is indicated.

discussed with the hypothetical MAR system, this zonation is also apparent deeper in the aquifer. Because of the higher horizontal than vertical flow velocities away from the pond, temperatures in this warm water zone are higher lateral away from the pond, than in the deeper part of the aquifer. The July calculation shows the same but reverse situation. The cross-section through the western pond is located at wells 10 and 11. Therefore, two well positions are shown in the left (northern) part of the cross-section. The pattern discussed with the horizontal cross-section is visible in the entire upper part of the aquifer. Notice however, that the zones influenced by older infiltration water temperature are mainly present in the shallow part of the aquifer and disappear deeper in the aquifer. Lower vertical than horizontal velocities and conduction of heat limit the vertical extension of these zones.

3.5. Temperature and residence times in the St-André MAR system

Sixteen thousand and eight hundred particles were placed at the location of the infiltration pond and were tracked to the extraction wells. Based on the particles travel time between pond and the different wells, a cumulative distribution of residence times was determined. This distribution indicates when water, recharged at the same instance, reaches the extraction well. Cumulative distributions were calculated for water infiltrated during winter and during summer. It was repeated twice: one with and one without taking into account heat transport (Fig. 12). The latter case is necessary to evaluate the effect of varying infiltration and extraction rates only.

Fig. 12 shows an important difference between cumulative frequency of residence times in case of winter or summer infiltration. If heat transport is not taken into account, 50% of the infiltrated water is extracted after 90.5 days for winter infiltration whereas this is 62.5 days for summer infiltration. Because of the higher infiltration and extraction rates during summer compared to those during winter (a factor of 1.6 and 1.4 respectively), there is a larger flow velocity to the extraction wells. However, the difference between cumulative frequency of winter and summer infiltration becomes smaller for larger residence times (more than 250 days) and is almost the same for residence times larger than 600 days. These larger residence times are influenced by infiltration and extraction rates during both summer and winter and their differences are averaged. Smaller residence times are only influenced by summer or winter conditions resulting in the differences calculated in the cumulative frequencies. Considering heat transport gives a slightly

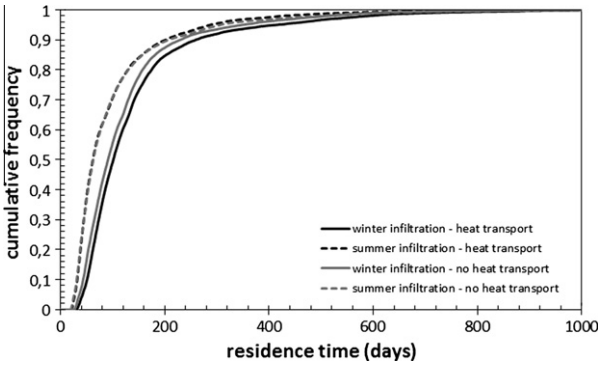

Fig. 12. Cumulative distribution of residence times of water infiltrated during winter and summer considering or neglecting heat transport.

different picture. 50% of the infiltrated water is extracted after 100.5 days for winter infiltration or 10 days later than not taking into account heat transport. This is 61.5 days or 1 day earlier for summer infiltration.

The different influence of heat transport during summer and winter infiltration is complex and varied. As indicated by the hypothetical MAR systems, infiltration and extraction rates, their ratio, location of extraction wells and seasonally varying rates all interfere. The St-André MAR system forms a combination of all those factors. During winter (December to March), ratio of extraction to infiltration rate is high, 1.5, and the absolute values are smallest (1.6×10^6 m^3 per month extraction and 1.05×10^6 m^3 per month infiltration). During summer, ratio of extraction to infiltration rate is lower, 1.3, and the absolute values are larger (2.2×10^6 m^3 per month extraction and 1.75×10^6 m^3 per month infiltration). Secondly, distance from wells to the pond ranges from 30 to 150 m. 75% of the wells are located at a distance which is less than 60 m from the ponds. Influence of well distance is illustrated by the median residence time for summer and winter infiltration in wells 60 and 85 (Table 6). Well 60 is at a distance of 35 m from the pond whereas this is 65 m for well 85. Well 60 shows a very small difference between median residence time considering and not considering heat transport for summer infiltration. Winter infiltration has a difference and this agrees with the result of the integrated extraction water. Well 85, illustrating a larger distance from the pond, is different. Both summer and winter infiltration shows a

Table 6
Median residence time for winter and summer infiltration (m_w and m_s) considering heat transport and for winter and summer infiltration not considering heat flow ($m_{0,w}$ and $m_{0,s}$), phase difference between temperature variations in the pond and the extraction wells for water infiltrated during winter ($\Delta\varphi_w$) and summer ($\Delta\varphi_s$) in wells 60 and 85 and the total extraction water.

	m_w (d)	m_s (d)	$m_{0,w}$ (d)	$m_{0,s}$ (d)	$\Delta\varphi_w$ (d)	$\Delta\varphi_s$ (d)
Extraction water	89	57	86.5	60	133	104
Well 60	54.5	35	48	34	93	53
Well 85	124	81	115	77	217	175

difference comparing taking into account heat transport or not taking into account the heat transport. Notice that the extraction water show intermediate values being a mean value for different wells with different distances to the pond.

Retardation of heat transport is calculated for the total extraction water. A phase difference of 133 (winter infiltration) and 104 (summer infiltration) days for the extraction water (Table 5) is calculated. This corresponds well with the observed phase difference of 110 days derived from the observations (Table 5). Because of the limited number of observation points in time, no distinction could be made between winter and summer. Calculated phase differences results in a retardation of 1.5 and 1.8 for winter and summer infiltration respectively. Individual wells also show a variation. Well 60 has an importantly smaller phase difference than well 85. Moreover, the calculated retardation is 1.7 and 1.5 for winter and summer infiltration respectively. For well 85, calculated retardation is 1.8 and 2.1 for winter and summer infiltration respectively. As for the hypothetical MAR systems, this illustrates that temperature provides only a rough proxy for residence times.

4. Conclusions

Seasonal variation of infiltration water temperature results in a temperature zonation in the aquifer. During winter, cold water is present in the aquifer under the pond. Farther from the pond, pore water is influenced by warmer water infiltrated during the previous summer. In many circumstances, influences of the previous winter infiltration of cold water persists also. A similar but opposite zonation is present in summer. Natural recharge and seasonally varying atmospheric temperature results in a similar zonation. This is for instance exemplified here by P19 and WP7. However temperature variations are much smaller than in case of higher artificial infiltration (e.g. ; Suzuki, 1960; Stallman, 1965; Vandenbohede and Lebbe, 2010).

Because of the high flow velocities during infiltration, impact of artificial recharge on the temperature in the aquifer is very significant. However, this influence is restricted to the immediate vicinity of the pond. In case extraction wells are located around the ponds, as we considered in this paper, influence on groundwater temperature of the aquifer outside the extraction well battery decreases very quickly. This is evident from the simulations with the hypothetical MAR systems, observations in WP7 of the St-André MAR system and the simulation of the latter system. Placing the extraction wells deeper or lowering the extraction to infiltration ratio for a given system, increases the temperature influence outside the well battery but still remains limited to the immediate vicinity of the MAR system.

Temperature influence of the pond is most important in the upper part of the aquifer and diminish relatively quickly deeper in the aquifer in case of shallow extraction wells. Conduction of heat and the fact that horizontal velocity to the extraction wells is higher than vertical velocity explains this. In case of a deeper extraction well, vertical influence of the artificial recharge increases.

Heat conduction smoothens the temperature variations in the aquifer. Close to the pond and in the shallow part of the aquifer, short-term temperature variations of the infiltration water persist. Deeper and farther from the pond these variations are smoothened and only a sinusoidal varying temperature variation is recorded as illustrated by the observations wells of the St-André MAR system.

Temperature variations influence hydraulic conductivity and this results in a larger infiltration capacity in summer than in winter. In case of the St-André system, this results in an 1.7 increase. Varying hydraulic conductivity influences residence time of infiltrated water. Pond water infiltrated during summer has in general a shorter residence time than pond water infiltrated in winter. A number of factors such as extraction to infiltration ratio, extraction and infiltration rates, location of extraction wells (distance to pond and depth) and seasonal variations in extraction and infiltration rates influences this. In general, residence time of water infiltrated during summer decreases and water infiltrated during winter increases because of the effect of temperature on hydraulic conductivity. But this is no general rule as shown by scenario 5 of the hypothetical MAR. The St-André MAR system shows the complexity because of varying seasonal extraction and infiltration rates and different distances to the pond for individual wells.

Hypothetical and St-André MAR systems have shown that temperature is only a rough proxy for the estimation of residence times of infiltrated water in the aquifer. If heat transport parameters are known as supposed in this paper, and observation of temperature variations in individual wells or the total extraction water are available, this provides only an estimate for the residence times of non-reactive advective transport. Main reason is the important conduction of heat smoothen temperature gradients.

Acknowledgements

AVDB is supported by the Fund for Scientific Research – Flanders (Belgium) where he is currently a postdoctoral fellow. Guy Vasseur and three anonymous reviewers are acknowledged for their constructive remarks and questions.

Appendix A. Supplementary material

Supplementary data associated with this article can be found, in the online version, at http://dx.doi.org/10.1016/j.jhydrol.2012.09.028.

References

Anderson, M.P., 2005. Heat as a ground water tracer. Ground Water 43 (6), 951–968.
Baveye, P., Vandevivere, P., Hoyle, B.L., De Leo, P.C., Sanchez de Lozada, D., 1998. Environmental impact and mechanisms of the biological clogging of saturated soils and aquifer materials. Crit. Rev. Environ. Sci. Technol. 28 (2), 123–191 (CRC Press).
Bouwer, H., 2002. Artificial recharge of groundwater: hydrogeology and engineering. Hydrogeol. J. 10, 121–142.
Constantz, J., 1998. Interaction between stream temperature, streamflow, and groundwater exchanges in alpine streams. Water Resour. Res. 34 (7), 1609–1616.
Constantz, J., Thomas, C.L., 1997. Streambed temperatures profiles as indicators of percolation characteristics beneath arroyos in the Middle Rio Grande Basin, USA. Hydrologic. Processes 11 (12), 1621–1634.
Constantz, J., Thomas, C.L., Zellwege, G., 1994. Influence of diurnal variations in stream temperature on streamflow loss and groundwater recharge. Water Resour. Res. 30 (12), 3253–3264.
Dausman, A.M., Langevin, C.D., Thorne, D.T., Sukop, M.S., 2010. Application of SEAWAT to select variable-density and viscosity problems. In: deMarsily, G. (Ed.), USGS Scientific Investigations Report 2009-5028, 1986. Quantitative Hydrogeology. Academic Press, San Diego, California.
Eusuff, M., Lansey, K., 2004. Optimal operation of artificial groundwater recharge systems considering water quality transformations. Water Resour. Manage. 18, 379–405.
Gooren, O., Gavrieli, I., Burg, A., Lazar, B., 2011. Cation exchange and $CaCO_3$ dissolution during artificial recharge of effluent to a calcareous sandstone aquifer. J. Hydrol. 400, 165–175.

Greskowiak, J., Prommer, H., Massmann, G., Johnston, C.D., Nützmann, G., Pekdeger, A., 2005. The impact of variably saturated conditions on hydrogeochemical changes during artificial recharge of groundwater. Appl. Geochem. 20, 1409–1426.

Harbaugh, A.W., Banta, E.R., Hill, M.C., McDonald, M.G., 2000. MODFLOW-2000, The US Geological Survey Modular Ground-Water Model: User Guide to Modularization Concepts and the Ground-Water Process. US Geol. Surv. Open-File Rep 00-92.

Hoffmann, A., Gunkel, G., 2011. Bank filtration in the sandy littoral zone of Lake Tegel (Berlin): structure and dynamics of the biological active filter zone and clogging processes. Limnologica 41 (1), 10–19.

Jaynes, D.B., 1990. Temperature variations effects on field measured infiltration. J. Soil Sci. Soc. Am. 54 (2), 305–312.

Konikow, L.F., Bredehoeft, J.D., 1978. Computer Model of Two-Dimensional Solute Transport and Dispersion in Ground Water. US Geological Survey Water-Resources Investigations Book 7 (Chapter C2).

Langevin, C.D., Thorne, D.T., Dausman, A.M., Sukop, M.C., Guo, W., 2007. SEAWAT Version 4: A Computer Program for Simulation of Multi-Species Solute and Heat Transport. US Geol. Surv. Tech. Methods, Book 6, Chap. A22. US Geological Survey Reston, VA.

Langevin, C.D., Dausman, A.M., Sukop, M.C., 2010. Solute and heat transport model of the Henry and Hilleke laboratory experiment. Ground Water 48 (5), 757–770.

Lebbe, L., 1973. Hydrogeologisch onderzoek van het duingebied te Oostduinkerke. (Hydrogeological study of the dune area at Oostduinkere, in Dutch). M.Sc. Dissertation. Ghent University.

Maeng, S.K., Sharma, S.K., Lekkerkerker-Teunissen, K., Amy, G.L., 2011. Occurrence and fate of bulk organic matter and pharmaceutically active compounds in managed aquifer recharge: a review. Water Res. 45 (10), 3015–3033.

Massmann, G., Greskowiak, J., Dünnbier, U., Zuehlke, S., Knappe, A., Pekdeger, A., 2006. The impact of variable temperatures on the redox conditions and the behaviour of pharmaceutical residues during artificial recharge. J. Hydrol. 328, 141–156.

Massmann, G., Sultenfuss, J., Dünnbier, U., Knappe, A., Taute, T., Pekdeger, A., 2008. Investigation of groundwater a residence times during bank filtration in Berlin: multi-tracer approach. Hydrologic. Processes 22 (6), 788–801.

Parsons, M.L., 1970. Groundwater thermal regime in a glacial complex. Water Resour. Res. 6 (6), 1701–1720.

Prommer, H., Stuyfzand, P.J., 2005. Identification of temperature-dependent water quality changes during a deep well injection experiment in a pyritic aquifer. Environ. Sci. Technol. 39, 2200–2209.

Rorabaugh, M.I., 1956. Ground Water Northeastern Louisville, Kentucky with Reference to Induced Infiltration. Water-Supply Paper 1360-B. USGS, Washington DC.

Schmidt, C.M., Fisher, A.T., Racz, A.J., Lockwood, B.S., Los Huertos, M., 2011. Linking denitrification and infiltration rates during managed groundwater recharge. Environ. Sci. Technol. 45, 9634–9640.

Sharme, L., Greskowiak, J., Chittaranjan, R., Eckert, P., Prommer, H., 2012. Elucidating temperature effects on seasonal variations of biogeochemical turnover rates during riverbank filtration. J. Hydrol. 42429, 104–105.

Slichter, C.S., 1905. Field Measurements of the Rate of Movement of Underground Waters. Water-Supply and Irrigation Paper No. 140. USGS, Washington, DC.

Stallman, R.W., 1963. Computation of Groundwater Velocity from Temperature Data. USGS Water Supply Paper 1544-H, pp. 36–46.

Stallman, R.W., 1965. Steady-one dimensional fluid flow in a semi-infinite porous medium with sinusoidal surface temperature. J. Geophys. Res. 70 (12), 2821–2827.

Stuyfzand, P.J., 1998. Fate of pollutants during artificial recharge and bank filtration in the Netherlands. In: Peters, (Eds.), Artificial Recharge of Groundwater. Balkema Rotterdam, pp. 119–125.

Stuyfzand, P.J., Segers, W., van Rooijen, N., 2007. Behavior of pharmaceuticals and other emerging pollutants in various artificial recharge systems in The Netherlands. In: Fox, P. (Ed.), Management of Aquifer Recharge for Sustainability, Proc. ISMAR-6, 28 Oct–2 Nov 2007, Phoenix AR USA. Acacia Publ. Inc., Phoenix, pp. 231–245.

Suzuki, S., 1960. Percolation measurements based on heat flow through soil with special reference to paddy fields. J. Geophys. Res. 65 (9), 2883–2885.

Thorne, D., Langevin, C.D., Sukop, M.C., 2006. Addition of simultaneous heat and solute transport and variable fluid viscosity to SEAWAT. Comput. Geosci. 32, 1758–1768.

van Breukel, B.M., Appelo, C.A.J., Olsthoorn, T.N., 1998. Hydrogeochemical transport modeling of 24 years of Rhine water infiltration in the dunes of the Amsterdam Water Supply. J. Hydrol. 209, 281–296.

Van Houtte, E., Verbauwhede, J., 2005. Artificial recharge of treated wastewater effluent enables sustainable groundwater management of a dune aquifer in Flanders, Belgium. In: Unesco (2006), Recharge Systems for Protecting and Enhancing Groundwater Resources. Proceedings of the 5th International Symposium on Management of Aquifer Recharge ISMAR5, Berlin, Germany, 11–16 June 2005. IHP-VI, Series on Groundwater No. 13, pp. 236–243.

Van Houtte, E., Verbauwhede, J., 2008. Operational experience with indirect potable reuse at the Flemish coast. Desalination 218 (2008), 198–207.

Vandenbohede, A., Lebbe, L., 2003. Combined interpretation of pumping and tracer tests: theoretical considerations and illustration with a field test. J. Hydrol. 277 (1–2), 134–149.

Vandenbohede, A., Lebbe, L., 2006. Occurrence of salt water above fresh water in dynamic equilibrium in coastal groundwater flow systems. Hydrogeol. J. 14 (4), 462–472.

Vandenbohede, A., Lebbe, L., 2010. Parameter estimation based on vertical heat transport in the surficial zone. Hydrogeol. J. 18, 931–943.

Vandenbohede, A., Lebbe, L., 2011. Heat transport in a coastal groundwater flow system near De Panne, Belgium. Hydrogeol. J. 19 (6), 1225–1238.

Vandenbohede, A., Van Houtte, E., Lebbe, L., 2008. Groundwater flow in the vicinity of two artificial recharge ponds in the Belgian coastal dunes. Hydrogeol. J. 16, 1669–1681.

Vandenbohede, A., Van Houtte, E., Lebbe, L., 2009a. Water quality changes in the dunes of the western Belgian coastal plain due to artificial recharge of tertiary treated wastewater. Appl. Geochem. 24, 370–382.

Vandenbohede, A., Van Houtte, E., Lebbe, L., 2009b. Sustainable groundwater extraction in coastal areas: a Belgian example. Environ. Geol. 57, 735–747.

Voss, C.I., 1984. A Finite-Element Simulation Model for Saturated–Unsaturated, Fluid-Density-Dependent Ground-Water Flow with Energy Transport or Chemically-Reactive Single-Species Solute Transport. US Geological Survey Water Resources Investigations Report 84-4369.

Wang, H.F., Anderson, M.P., 1982. Introduction to Groundwater Modeling. Finite Difference and Finite Element Methods. Freeman, San Francisco.

Wiese, B., Massmann, G., Jekel, M., Heberer, T., Dunnbier, U., Orlikowski, D., Grutzmacher, G., 2011. Removal kinetics of organic compounds and sum parameters under field conditions for managed aquifer recharge. Water Res. 45 (16), 4939–4950.

Winslow, J.D., 1962. Effect of Stream Infiltration on Ground Water Temperatures Near Schenectady. NY USGS Professional Paper 450-C. USGS, Washington, DC.

Zheng, C., Wang, P.P., 1999. MT3DMS, a Modular Three-Dimensional Multispecies Model for Simulation of Advection, Dispersion and Chemical Reactions of Contaminants in Groundwater Systems: Documentation and User's Guide. US Army Engineer Research and Development Center Contract Report SERDP-99-1. USAERDC, Vicksburg, MI.